A Novel Bioinspired Tracking Control Method for Mobile Robots with the Adaptive Sliding Innovation Filter

Zhe Xu[a], Waleed Hilal[a], S. Andrew Gadsden[a], and Mohammad Al-Shabi[b]

[a]McMaster University, Hamilton, Canada
[b]University of Sharjah, Sharjah, United Arab Emirates

ABSTRACT

This paper developed a hybrid tracking control strategy for mobile robots based on a bioinspired neurodynamics. The proposed control method addresses the tracking control problem of mobile robots that considers the speed jump issue, velocity constraint, disturbances, and noises. In addition, considering the accuracy of the state estimates, an adaptive sliding innovation filter is integrated with the control. Compared to the conventional control approach, the proposed control strategy provides bounded smooth velocity and torque control inputs without velocity jump yet robust to disturbances. The adaptive sliding innovation filters that are integrated with the proposed control strategy not only provide accurate state estimates but are robust to modeling uncertainties as well. Finally, the simulation results demonstrate the overall control performance of the proposed method.

Keywords: Adaptive estimation, bioinspired neural dynamics, control theory, estimation theory, mobile robots, robust estimation, sliding innovation filter, target tracking

1. INTRODUCTION

Tracking control of mobile robots has always been an interesting topic in robotics due to its vast applications, such as transportation, military, and surveillance. In real-world applications, autonomous mobile robots are usually deployed in complex environments that pose threat to human beings, thus, various factors such as disturbances and noises have huge impact on the control performance. On the other hand, due to the physical limitations of the robots, the speed jump issue and velocity constraints are also critical issues. Thus, the development of an effective control method for mobile robots is quite challenging by considering these realistic factors.

There have been various studies related to robot tracking control, these control strategies can be mainly categorized into feedback linearization control,[1,2] fuzzy logic control[3,4] and neural networks,[5–7] sliding mode control[8,9] and backstepping control.[10–12] In terms of the estimation strategy for robot systems working under system and measurement noises, there are many filters and its variations have been developed such as Kalman filter (KF),[13–16] extended Kalman filter[9,17,18] (EKF), Unscented Kalman filter (UKF).[19–21]

The linearization method uses a decoupling matrix to linearize the nonlinearities within of the system, although this method is straightforward, in order for this method to work, the initial tracking error should be small, otherwise, there will be a speed jump at the initial stage, which requires the robot actuator to yield an impractical amount of torque to achieve initial velocity. Fuzzy logic control is a practical solution that resolves the impractical speed jump; however, this method is relatively difficult to set up fuzzy rules because it requires errors and trials based on human knowledge and experiences. Neural networks is able to resolve the speed jump issue; however, this method requires online learning, which is time consuming. Backstepping control is a simple solution for mobile robot control that is relatively easy to design and proven by the Lyapunov stability theory, however, this method also suffers from speed jump issue due to its control terms that is embedded in its design. Sliding mode control is a well-developed method for robot control, it can reduce the initial speed jump if tracking error occurs; however, it cannot completely avoid such jump. In addition, the sliding-mode control is knowingly

Further author information: (Send correspondence Zhe Xu or S.A. Gasden)
Z.X: E-mail: xu804@mcmaster.ca
S.A.G: E-mail: gadsden@mcmaster.ca

Autonomous Systems: Sensors, Processing, and Security for Ground, Air, Sea, and Space Vehicles and Infrastructure 2024, edited by Michael C. Dudzik, Stephen M. Jameson, Theresa J. Axenson, Proc. of SPIE Vol. 13052, 1305209 · © 2024 SPIE · 0277-786X · doi: 10.1117/12.3013754

suffering from a chattering issue, which makes this method hard to implement on a real robot without any modifications. Yang *et. al.*[11] has solved the speed jump problem using a backstepping approach that is integrated with bioinspired neural dynamics.

On the other hand, the robot usually operates in complex environments, where disturbances and noises play critical roles in the tracking performance. The sliding mode control is a promising approach that is capable of dealing with disturbances.[22,23] However, the sign function in the control design makes the control inputs suffer from chattering problems. To address the chattering issue, the commonly used approach is to use the saturation function, which replaces the sign function. Although this approach avoids the chattering problem, when a mobile robot operates under high-frequency noises, the smoothness of control inputs is doubtful to be implementable on a real robot.

Since autonomous robots usually operate in noisy environments, the state estimation and tracking accuracy are heavily affected by noises. Therefore, multiple estimation techniques have been introduced to provide accurate state estimates under noises. Filters, such as Kalman filter,[24,25] extended Kalman filter,[26] and Unscented Kalman filter[19] have a vast usage in real-world applications; these filters are efficient approaches to provide accurate state estimates under noises if systems have no modeling errors, while in real world situations, modeling of the mobile robot could be impacted by various conditions such as material abrasion, wheel worn, disturbances. Therefore, considering modeling errors, these approaches may fail to provide accurate state estimates; it is found that an adaptive sliding innovation filtering method was recently proposed to address the robust estimation problem yet maintain the robustness of state estimation strategy.[27,28]

Followed by previous work,[11,29] this paper not only aims to resolve the speed jump issue in backstepping control within robot kinematics but also develop a sliding mode control that is robust to disturbances smooth bounded control input. In addition, in real-world applications, the mobile robot usually works in noisy environments that may have modeling errors if the robot is ill-conditioned, which leads to inaccurate state estimates. Thus, this paper aims to directly tackle these problems and develop a hybrid control strategy that considers speed jump and chattering issues, control smoothness, and modeling error due to the noises and ill conditioned robot. The main contributions of this paper are listed as follows,

1) A bioinspired sliding mode control of a mobile robot is proposed, which is free from chattering with smooth control input under the effects of noises. The proposed bioinspired sliding mode method is capable of reducing the initial torque demand when velocity tracking error occurs; more importantly, with the presence of system noises, the proposed control is capable of providing smooth torque control input.

2) Considering the speed jump issue in conventional backstepping control, a combination of bioinspired backstepping and sliding mode control strategy is proposed, which not only resolves the speed jump issue and provides smooth velocity and torque control inputs when noises occur.

3) Since the system and measurement noises have huge impacts on tracking performance, an adaptive sliding innovation filter is integrated with the bioinspired hybrid control strategy. The ASIF and AESIF provide accurate state estimates and offer extra robustness to modeling errors. The overall control strategy has improved the control performance of mobile robots that work in difficult conditions and provides accurate state estimates.

This paper is organized as follows, Section II models the kinematics and dynamics of a mobile robot as well as introducing the ASIF and AESIF. Section III develops the bioinspired hybrid control strategy that is integrated with ASIF and EASIF. Section IV presents the simulation results that demonstrate the efficiency and effectiveness of the proposed control strategy in multiple scenarios. Section V draws conclusions with respect to the overall control strategy.

2. MODELING OF A MOBILE ROBOT

This section formulates the kinematic and dynamic model of a nonholonomic differential drive wheeled mobile robot in a 2-dimensional Cartesian workspace. As seen from Figure1, X, O, Y and D, P_c, L are the localization of the mobile robot in inertial and body fixed frame, respectively; $2l$ is the distance between two wheels; $2c$ is the diameter of the driving wheels; P_0 denotes the center of mass; P_c is the reference point of the body fixed frame. The position and orientation angle of the mobile robot is given as $P_a = [x_a, y_a, \theta_a]^T$ in the inertial frame.

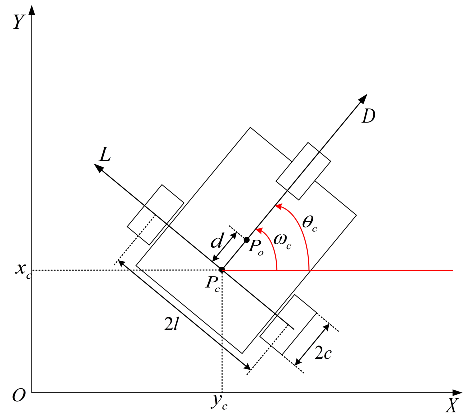

Figure 1. Schematic of mobile robot.

2.1 Kinematics and dynamics of mobile robots

For the kinematic of a nonholonomic mobile robot, assume there is no slipping condition, its kinematic constraint is provided as

$$A(P_a)\dot{P}_a = \dot{y}_a \cos\theta_a - \dot{x}_a \sin\theta_a - d\dot{\theta}_a = 0 \tag{1}$$

where $A(p)$ is the constraint matrix. In terms of the motion control, the nonholonomic mobile robots involves two degrees of freedom, which are the linear velocity υ_a and angular velocity ω_a. The relations between υ_a, ω_a with respect to the velocity of the mobile robot in the inertial frame is calculated through a Jacobian matrix as

$$\begin{aligned}
&\dot{P}_a = J(P_a)\xi_a \\
&J(P_a) = \begin{bmatrix} \cos\theta_a & -d\sin\theta_a \\ \sin\theta_a & d\cos\theta_a \\ 0 & 1 \end{bmatrix} \qquad \xi_a = \begin{bmatrix} \upsilon_a \\ \omega_a \end{bmatrix}
\end{aligned} \tag{2}$$

As for the dynamics of the mobile robot, the general Euler-Lagrangian equation is given as

$$M(P)\ddot{P} + C(P,\dot{P})\dot{P} + \tau_d = B(P)\tau - A^T(P)\lambda \tag{3}$$

where $M(P)\ddot{P}$ is a symmetric, positive definite inertia matrix; $C(p,\dot{p})$ represents the centrifugal and Coriolis effects, $B(P)$ is the transformation matrix; and τ_d is the disturbances. Variable $\tau = [\tau_L, \tau_R]$ represents the input torque from left and right wheels, λ is the constraint force. From the control perspective, the state space model of the mobile robot can be developed by integrating the kinematics and dynamics to improve the control efficiency. By taking the time derivative of (2), it can be calculated that

$$\ddot{P}_a = \dot{J}(P_a)\xi_a + J(P_a)\dot{\xi}_a \tag{4}$$

Then, multiply (3) by $J(P_a)^T$ and combine with (4), it is calculated that

$$\bar{M}(P)\dot{\xi}_a = \bar{B}(P_a)\tau - \bar{C}(P_a,\dot{P}_a)\xi_a \tag{5}$$

Variables $\bar{M}(P)$, $\bar{C}$, and $\bar{B}(P)$ are calculated as

$$\begin{aligned}
&\bar{M}(P_a) = J(P_a)^T M J(P_a) \\
&\bar{C}(P_a,\dot{P}_a) = J(P_a)^T \left(M(P_a)\dot{J}(P_a) + C(P,\dot{P}_a)J(P_a) \right) \\
&\bar{B}(P_a) = J(P_a)^T B(P_a)
\end{aligned} \tag{6}$$

These parameters are given by

$$\begin{aligned}
&\bar{\mathrm{M}} = \begin{bmatrix} m & 0 \\ 0 & I - md^2 \end{bmatrix} \bar{\mathrm{C}} = \begin{bmatrix} 0 & 0 \\ 0 & 0 \end{bmatrix} \\
&\bar{\mathrm{B}} = \frac{1}{r}\begin{bmatrix} 1 & 1 \\ l & -l \end{bmatrix} \tau_c = \begin{bmatrix} \tau_R \\ \tau_L \end{bmatrix}
\end{aligned} \tag{7}$$

where and m is the mass of the mobile robot, I is the moment of inertia, r is the radius of the left and right wheels, τ_L and τ_R represent the torque, which are generated from DC motors to the left and right driving wheels. In this paper, the origin point of the body fixed frame is set to be the same as the center of gravity of the mobile robot, which refers to $d = 0$.

2.2 Error Dynamics

The consensus error of i-th mobile robot is defined as A path planner first generates the desired position and orientation of the mobile robot, which is defined as $P_d(t) = [x_d(t), y_d(t), \theta_d(t)]^{\mathrm{T}}$. Defining e_1, e_2, and e_3 as the tracking errors of driving, lateral directions, and orientation with respect to the body fixed frame. Then, through a transformation matrix the relations of tracking error between the inertial frame and body fixed frame are obtained as

$$e_P = \begin{bmatrix} e_1 \\ e_2 \\ e_3 \end{bmatrix} = \begin{bmatrix} \cos\theta_c & \sin\theta_c & 0 \\ -\sin\theta_c & \cos\theta_c & 0 \\ 0 & 0 & 1 \end{bmatrix} \begin{bmatrix} e_x \\ e_y \\ e_\theta \end{bmatrix} \tag{8}$$

where e_x, e_y, and e_θ are the tracking error of X, Y, and orientation θ directions and they are defined as $e_x = x_d - \hat{x}_a$, $e_y = y_d - \hat{y}_a$. Then, the error dynamics is calculated from (8) as

$$\begin{bmatrix} \dot{e}_1 \\ \dot{e}_2 \\ \dot{e}_3 \end{bmatrix} = \begin{bmatrix} \omega_c e_2 - \upsilon_c + \upsilon_d \cos e_3 \\ -\omega_c e_1 + \upsilon_d \sin e_3 \\ \omega_d - \omega_c \end{bmatrix} \tag{9}$$

where υ_d and ω_d are the respected desired linear and angular velocity, which is given as

$$\upsilon_d = \sqrt{x_d{}^2 + y_d{}^2} \tag{10}$$

$$\omega_d = \frac{\ddot{y}_d \dot{x}_d - \ddot{x}_d \dot{y}_d}{\dot{x}_d^2 + \dot{y}_d^2} \tag{11}$$

2.3 Kalman filter

The KF was developed in 1960s, this filter provides optimal states estimates for linear system, which the design of KF is described as follows For a linear system that is descirbed as

$$x_{k+1} = Ax_k + Bu_k + \gamma_k \tag{12}$$

$$z_{k+1} = Cx_{k+1} + \delta_{k+1} \tag{13}$$

where $\hat{x}_k$ and $\hat{x}_{k+1}$ are the state of the system at time step k and $k+1$, respectively, z_{k+1} is the measurement of the state; A and B are respectively the system and input matrices; γ and δ are respectively the system and measurement noises, which both are regarded as zeros mean Gaussian. It is assumed that the system is linear well known in order for the filter to provide accurate state estimates. In addition, the noise covariances are also assumed to be known in order for the filter to be worked properly. The KF is firstly processed through the predicting stage, which is illustrated in three equations

$$\hat{x}_{k+1|k} = A\hat{x}_{k|k} + Bu_k \tag{14}$$

$$P_{k+1|k} = AP_{k|k}A^T + R_k \tag{15}$$

where R_k is the system noise covariance; x_k and x_{k+1} are the state of the system at time step k and $k+1$; $P_{k+1|k}$ and $P_{k|k}$ is the error matrix predicted and posterior state error covariance matrices, respectively. After $\hat{x}_{k+1|k}$ and $P_{k+1|k}$ are calculated, the KF goes through the update stage, which updates the updated state estimates $\hat{\mathrm{x}}_{k+1|k+1}$, the Kalman gain K_{k+1} and updated state error covariance matrix $P_{k+1|k+1}$

$$K_{k+1} = P_{k+1|k}C^T[CP_{k+1|k}C^T + Q_{k+1}]^{-1} \tag{16}$$

$$\hat{x}_{k+1|k+1} = \hat{x}_{k+1|k} + K_{k+1}[z_{k+1} - C\hat{x}_{k+1|k}] \tag{17}$$

$$P_{k+1|k+1} = [I - K_{k+1}C]P_{k+1|k} \tag{18}$$

where Q_k is the measurement noise covariance. The KF provides optimal states estimates if the system is well known and without considering any uncertainties. In addition, the KF does not have the robustness against faulty data that is caused by modeling errors and uncertainties, which could potentially have a huge impact on the control performance.

2.4 ASIF and AESIF

Autonomous robots have been widely used in environments that could be dangerous in the presence of human beings, such as radiation, biohazrd, etc. Therefore, the complexity of the environment could also yield system and measurement noises that affect the control performance of the robot. Thus, it is necessary for robot to equip efficient and effective estimators that reduce these noises and provide accurate state estimates. Although there are various estimate strategies that provides state estimates such as KF for linear system, UKF, EKF, and CKF. These filters lack of robustness, in other words, when there are modelling errors in which faulty date being processed in the mobile robot, the aforementioned filters fail to provide accurate state estimates that could pose dangerous and loss control capability. The SIF is a newly proposed filter that is based on Kalman gain, compared with KF and other filters, this filter is robust to disturbances and model uncertainties due to its switching gain. Considering the working conditions of the autonomous system, having a filter with more robustness is rather critical in real world applications. The design of the conventional SIF is similar to the KF, which is based on a predictor-corrector estimation method. The following part illustrates the design procedures of the SIF A linear system is firstly processed through a predict stage, which is given as

$$\hat{x}_{k+1|k} = A\hat{x}_{k|k} + Bu_k \tag{19}$$

$$P_{k+1|k} = AP_{k|k}A^T + R_k \tag{20}$$

$$\hat{z}_{k+1|k} = z_{k+1} + C\hat{x}_{k+1|k} \tag{21}$$

where $\hat{z}_{k+1|k}$ and $\hat{z}_k$ are the predicted and measured robot states; these updated variables are then processed through the update stage to provide updated state estimates. The updated state error covariance $P_{k+1|k+1}$ and updated state estimates $\hat{x}_{k+1|k+1}$ along with the updated sliding innovation gain $K_k + 1$ are calculated as

$$K_{k+1} = C^{+}\text{diag}(sat\left(\frac{\left|\hat{z}_{k+1|k}\right|}{\alpha}\right) \tag{22}$$

$$\hat{\mathrm{x}}_{k+1|k+1} = \hat{\mathrm{x}}_{k+1|k} + K_{k+1}\hat{z}_{k+1|k} \tag{23}$$

$$\begin{aligned} P_{k+1|k+1} = (I - K_{k+1}C)P_{k+1|k}(I- \\ K_{k+1}C)^T + K_{k+1}Q_{k+1}{K_{k+1}}^T \end{aligned} \tag{24}$$

where I is an identity matrix, C^{+} is the pseudoinverse of the measurement matrix, and sat refers to the saturation function, α is the width of the sliding boundary. Compared with the KF, the main differences is that the gain is calculated using the measurement matrix, the innovation and α for the sliding innovation filter while the KF uses the state error covariance. Since the SIF does not use state error covariance and sliding boundary α is manually tuned to provide the best possible results, therefore, it does not provide optimal state estimates as KF does. Thus, in order to improve the accuracy, the time vary sliding boundary and new sliding innovation gain is proposed as

$$S_{k+1} = CP_{k+1|k}C^T + Q_{k+1} \tag{25}$$

$$\alpha_{k+1} = S_{k+1}(S_{k+1} - Q_{k+1})^{-1}\text{diag}\left|\hat{z}_{k+1|k}\right| \tag{26}$$

$$K_{k+1} = C^{+}\text{diag}\left|\hat{z}_{k+1|k}\right|\alpha_{k+1}^{-1} \tag{27}$$

where S_{k+1} is the sliding innovation covariance. Thus, the time varying adaptive sliding innovation filter(ASIF is presented. This ASIF works for linear system and provide accurate state estimates as KF does, however, most real word robots are nonlinear system, therefore, the ESIF that works for the nonlinear system is introduced, given a typical nonlinear system

$$x_{k+1} = f(x_k, u_k) + \beta_k \tag{28}$$

$$z_{k+1} = c(x_{k+1}) + \varsigma_{k+1} \tag{29}$$

where $f(x_k, u_k)$ and $h(x_{k+1})$ represents the nonlinear mathematical calculation of the system and measurement model; β and ς are the system and measurement noises of the nonlinear system, respectively. Then, the ESIF requires the linearization of these nonlinearities using partial derivatives as

$$A_{f,k} = \left.\frac{\partial f}{\partial x}\right|_{\hat{\mathrm{x}}_{k|k,uk}} \tag{30}$$

$$C_{f,k+1} = \left.\frac{\partial c}{\partial x}\right|_{\hat{\mathrm{x}}_{k|k,uk}} \tag{31}$$

where $A_{f,k}$ and $C_{f,k+1}$ are the linearized system. Then, following the similar process of sliding innovation filter, the predict stage of the ESIF is shown as

$$\hat{\mathrm{x}}_{k+1|k} = f(\hat{x}_{k|k}, u_k) \tag{32}$$

$$P_{k+1|k} = A_{f,k} P_{k|k} A_{f,k}^T + G_k \tag{33}$$

$$\hat{z}_{k+1|k} = z_{k+1} + C_{f,k+1}(\hat{x}_{k+1|k}) \tag{34}$$

Then, $\hat{\mathrm{x}}_{k+1|k}$, $P_{k+1|k}$, and $\hat{z}_{k+1|k}$ are processed through the update stage to generate the estimated states along with the updated sliding innovation gain. The updated stage is demonstrated in three equations as

$$K_{k+1} = C_{f,k+1}^{+} \mathrm{diag}(\mathrm{sat}\left(\frac{\left|\hat{z}_{k+1|k}\right|}{\alpha}\right) \tag{35}$$

$$\hat{\mathrm{x}}_{k+1|k+1} = \hat{\mathrm{x}}_{k+1|k} + K_{k+1}\hat{z}_{k+1|k} \tag{36}$$

$$\begin{aligned} P_{k+1|k+1} = (I - K_{k+1}C_{f,k+1})P_{k+1|k}(I- \\ K_{k+1}C_{f,k+1})^T + K_{k+1}Q_{k+1}K_{k+1}{}^T \end{aligned} \tag{37}$$

where Q_{k+1} is the measurement noise covariances, this ESIF shares the similar function as the conventional sliding innovation filter as it is robust to the disturbances and modelling errors, again, in order for the ESIF to provide accurate state estimates, the sliding boundary and sliding innovation gain are changed to

$$S_{k+1} = C_{f,k+1} P_{k+1|k} C_{f,k+1}{}^T + Q_{k+1} \tag{38}$$

$$\alpha_{k+1} = S_{k+1}(S_{k+1} - Q_{k+1})^{-1}\mathrm{diag}\left|\hat{z}_{k+1|k}\right| \tag{39}$$

$$K_{k+1} = C_{f,k+1}^{+}\mathrm{diag}\left|\hat{z}_{k+1|k}\right| \alpha_{k+1}^{-1} \tag{40}$$

Then, the time vary adaptive extended sliding innovation filter (AESIF) is introduced, this filter not only able to provide accurate state estimates, but also robust to disturbances for nonlinear systems. For mobile robot working autonomously, the robustness and accuracy of estimator are both critical, ASIF and AESIF are capable of satisfying both criteria.

3. DESIGN OF BIOINSPIRED BASED CONTROLLER AND SLIDING INNOVATION FILTERS

This section designs the control strategy that is suitable for mobile robots work in complex environments where system and measurement noises take critical roles in tracking performance. Considering the disturbances, the ASIF and AESIF are firstly designed to provide accurate state estimates. Then, the bioinspired based backstepping and sliding mode control are designed to provide smooth velocity curve without speed jump and chattering issue, which make the proposed control more practical in real world applications. The overall control design schematic is shown in 2, which illustrates two closed loop control design for kinematics and dynamics. The detailed design procedure is demonstrated in the following subsections.

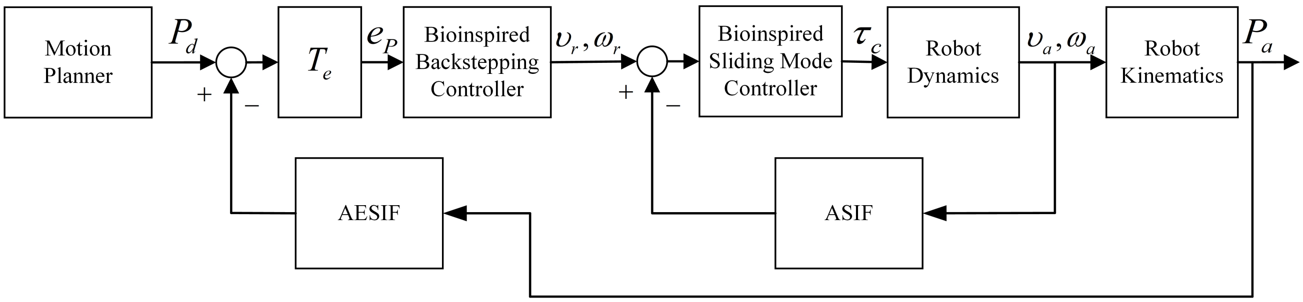

Figure 2. Block diagram of an UAV based on the bioinspired control strategy

3.1 Bioinspired neural dynamics

The applications of the bioinspired neural dynamic model, which describes a patch of membrane using electrical elements, was firstly introduced by Grossberg that was written as

$$\dot{y}_i = -A_i y_i + (B_i - x_i){S_i}^+ - (D_i + y_i){S_i}^- \tag{41}$$

where y_i is the output of the i-th neural activity; A_i is the passive decay rate; B_i and D_i are respectively the upper and lower bounds of the ith neural activity; ${S_i}^+$ and ${S_i}^-$ are respectively the excitatory and inhibitory inputs of i-th neuron. This shunting equation modeled the neural activity of the a single neuron that its neural activity is bounded into a finite interval $[-D_i, B_i]$ and can be rewritten in a more direct form as

$$\dot{\upsilon}_i = -A_i \upsilon_i + (B_i - \upsilon_i) f(e_i) - (D_i + \upsilon_i) g(e_i) \tag{42}$$

where υ_i is the output from the shunting equation; $f(e_i)$ and $g(e_i)$ are respectively defined as $\max(e_i, 0)$ and $\max(-e_i, 0)$. The bioinspired neural dynamics was first applied in robotics by Yang and Meng,[30] which was later expanded in various areas in robotics.[10,11] This shunting model has apparent advantages in that it not only bound the output between $[-D_i, B_i]$, but also acts as a low pass filter. Thus, inspired by these special characteristic of the shunting model, this paper aims to develop control strategies that are based on the shunting model which would help improve the control performance.

4. BIOINSPIRED CONTROLLER DESIGN

Autonomous mobile robots usually operate in complex environments where disturbances and noises have a huge impact on tracking performance. The proposed controller aims to provide smooth control inputs under noises while offering extra robustness against disturbances. The overall design is followed by a kinematic and a dynamic controller that is both integrated with the shunting model. To provide accurate state estimates under measurement noises, the adaptive sliding innovation filter is integrated with the proposed bioinspired control to provide accurate state estimates under modeling errors.

4.1 Kinematic control

The conventional backstepping kinematic control of the mobile robot is proposed as

$$\upsilon_r = k_1 e_1 + \upsilon_d \cos e_3 \tag{43}$$

$$\omega_r = \omega_d + k_2 e_3 + \frac{k_3 e_2 \upsilon_d \sin e_3}{e_3} \tag{44}$$

By observing the error term $k_1 e_1$ and $k_2 e_2$ within the conventional control design, it is noticed that the velocity jumps occur if e_1 and e_2 are not zeros. This impractical velocity jump implies that the torque demand that is required for the mobile robot to reach such velocities instantly will tend to be infinitely large. Thus, to avoid speed jump issues, the error term e_1 and e_3 are both replaced by the shunting model, and the bioinspired backstepping control is defined as

$$\upsilon_r = k_1 \upsilon_{s1} + \upsilon_d \cos e_3 \tag{45}$$

$$\omega_r = \omega_d + k_2 \upsilon_{s2} + \frac{k_3 e_2 \upsilon_d \sin e_3}{e_3} \tag{46}$$

where υ_{s1} and υ_{s2} are the output from the shunting model which is defined as

$$\frac{d\upsilon_{si}}{dt} = -A_i \upsilon_{si} + (B_i - \upsilon_{si}) f(e_i) - (D_i + \upsilon_s) g(e_i) \quad i = 1, 2 \tag{47}$$

where A_i, B_i and D_i are positive design constants; $f(e_i)$ and $g(e_i)$ are respectively defined as $\max\{e_i, 0\}$ and $\max\{-e_i, 0\}$.

Remark 1 Based on the observation of (45), the maximum linear velocity command is given by $k_1 B_1 + \upsilon_d$ regardless of the tracking error, therefore, the shunting model addresses the velocity constrain issue for the mobile robot.

Remark 2 The shunting model is a dynamic model, therefore, the outputs of the shunting model starts from 0 at the initial stage, thus preventing velocity jumps and provides smooth transition of the linear velocity.

To prove its stability, the Lyapunov candidate function is proposed as

$$V_1 = \frac{1}{2} {e_1}^2 + \frac{1}{2} {e_2}^2 + \frac{1}{2k_3} {e_3}^2 + \frac{k_1}{2B_1} {\upsilon_{s1}}^2 + \frac{k_2}{2k_3 B_2} {\upsilon_{s2}}^2 \tag{48}$$

Then, its time derivative $\dot{V}_1$ becomes

$$\dot{V}_1 = \dot{e}_1 e_1 + \dot{e}_2 e_2 + \frac{1}{k_3} \dot{e}_3 e_3 + \frac{k_1}{B_1} \dot{\upsilon}_{s1} \upsilon_{s1} + \frac{k_2}{k_3 B_2} \dot{\upsilon}_{s2} \upsilon_{s2} \tag{49}$$

By substituting (9) into (62), it is calculated that

$$\begin{aligned} \dot{V}_1 = {} & e_1(\omega_r e_2 - \upsilon_r + \upsilon_d \cos e_3) + e_2(-\omega_r e_1 + \upsilon_d \sin e_3) + \\ & \frac{1}{k_3}(\omega_d - \omega_r) e_3 + k_1 \upsilon_{s1}(-A_1 \upsilon_{s1} + (B_1 - \upsilon_{s1}) f(e_1) - \\ & (D_1 + \upsilon_s) g(e_1)) + \frac{k_2}{k_3} \upsilon_{s2}(-A_2 \upsilon_{s2} + (B_2 - \upsilon_{s2}) f(e_2) - \\ & (D_2 + \upsilon_{s2}) g(e_2)) \\ & = -k_1 \upsilon_{s1} e_1 - \frac{k_2}{k_3} \upsilon_{s2} e_3 + k_1 \upsilon_{s1}(-A_1 \upsilon_{s1} + (B_1 - \\ & \upsilon_{s1}) f(e_1) - (D_1 + \upsilon_s) g(e_1)) + \frac{k_2}{k_3} \upsilon_{s2}(-A_2 \upsilon_{s2} + (B_2 - \\ & \upsilon_{s2}) f(e_2) - (D_2 + \upsilon_s) g(e_2)) \end{aligned} \tag{50}$$

Then, by setting $B_1 = D_1$ and $B_2 = D_2$, $\dot{V}_1$ is written as

$$\begin{aligned} \dot{V}_1 = {} & \frac{k_1}{B_1} {\upsilon_{s1}}^2(-A_1 - f(e_1) - g(e_1)) + k_1 \upsilon_{s1}(-e_1 + f(e_1) - \\ & g(e_1)) + \frac{k_2}{k_3 B_2} {\upsilon_{s2}}^2(-A_2 - f(e_2) - g(e_2)) + \frac{k_2}{k_3} \upsilon_{s2}(- \\ & e_2 + f(e_2) - g(e_2)) \end{aligned} \tag{51}$$

Based on the definition of $f(e_i)$ and $g(e_i)$, it is easy to verify that

$$\upsilon_{si}(-e_i + f(e_i) - g(e_i)) = 0 \quad \text{for} \quad i = 1, 2 \tag{52}$$

Then, the rest of (51) is written as,

$$\begin{aligned} & \frac{k_1}{B_1} {\upsilon_{s1}}^2(-A_1 - f(e_1) - g(e_1)) + \frac{k_2}{k_3 B_2} {\upsilon_{s2}}^2(-A_2 - f(e_2) \\ & \qquad - g(e_2)) \leq 0 \end{aligned} \tag{53}$$

Thus, $\dot{V}_1 \leq 0$, which implies that $\dot{V}_{si} \to 0$ as $t \to \infty$, based on the input output properties of the shunting model defined in (42), if $\dot{V}_{si} \to 0$, then $e_1 \to 0$ and $e_3 \to 0$ as $t \to \infty$. Then, based on (46), $e_2 \to 0$ as well. Thus, the kinematic control at the equilibrium point $e_P = 0$ is asymptotically stable.

4.2 Dynamic controller

It is also critical to design a dynamic controller that is robust to disturbances. It is known that the sliding mode control is robust to disturbances, however, the practicality of this method is limited due to its chattering nature and control smoothness under noises. Therefore, this section develops a bioinspired sliding mode control to address these problems.

Define the error between the velocity commands from the kinematic controller and estimated velocity as

$$e_\eta = \begin{bmatrix} e_4 \\ e_5 \end{bmatrix} = \begin{bmatrix} \upsilon_r - \upsilon_a \\ \omega_r - \omega_a \end{bmatrix} \tag{54}$$

where e_4 and e_5 are respectively the linear and angular tracking errors; υ_a and ω_a are the linear and angular velocities, respectively. Then, the conventional sliding mode dynamic controller is given by

$$\tau_L = \frac{mr}{2}\left(\dot{\upsilon}_r + C_4 \text{sat}(e_4)\right) - \frac{Ir}{2l}(\dot{\omega}_r + C_5 \text{sat}(e_5)) \tag{55}$$

$$\tau_R = \frac{mr}{2}\left(\dot{\upsilon}_r + C_4 \text{sat}(e_4)\right) + \frac{Ir}{2l}(\dot{\omega}_r + C_5 \text{sat}(e_5)) \tag{56}$$

The saturation function is capable of avoiding the chattering issue to some extent; however, when there are high-frequency disturbances such as noises, the control smoothness cannot be guaranteed, thus, the practicability in the real-world application is limited. The bioinspired sliding mode controller aims to provide smooth control input free from chattering. Thus, by replacing the error terms within the sliding mode control, the bioinspired sliding mode torque control is proposed as

$$\tau_L = \frac{mr}{2}\left(\dot{\upsilon}_r + k_4 \upsilon_{s4}\right) - \frac{Ir}{2l}(\dot{\omega}_r + k_5 \upsilon_{s5}) \tag{57}$$

$$\tau_R = \frac{mr}{2}\left(\dot{\upsilon}_r + k_4 \upsilon_{s4}\right) + \frac{Ir}{2l}(\dot{\omega}_r + k_5 \upsilon_{s5}) \tag{58}$$

where υ_{s4} and υ_{s5} are respectively defined as

$$\frac{d\upsilon_{s4}}{dt} = -A_4 \upsilon_{s4} + (B_4 - \upsilon_{s4}) f(e_4) - (D_4 + \upsilon_{s4}) g(e_4) \tag{59}$$

$$\frac{d\upsilon_{s5}}{dt} = -A_5 \upsilon_{s5} + (B_5 - \upsilon_{s5}) f(e_5) - (D_5 + \upsilon_{s5}) g(e_5) \tag{60}$$

Remark 3 Since the shunting model shows its dynamic behavior, thus, it provides more consistent outputs considering the inputs e_4 and e_5. In contrast, the saturation function does not exhibit such dynamic behavior and causes discontinuities in control input when noises occur. In addition, the output of the shunting model is strictly bounded between $(-D_i, B_i)$, thus sharing similar properties as the saturation function, and is able to constrain the control output to a certain degree.

To prove the stability of the proposed controller, the Lyapunov candidate function is proposed as

$$V_2 = \frac{1}{2B_4} {e_4}^2 + \frac{1}{2B_5} {e_5}^2 + \frac{k_4}{B_4} \upsilon_{s4}^2 + \frac{k_5}{B_5} \upsilon_{s5}^2 \tag{61}$$

The time derivative of (61) becomes

$$
\begin{aligned}
\dot{V}_2 =& \frac{1}{B_4} e_4 \dot{e}_4 + \frac{1}{B_5} e_5 \dot{e}_5 + \frac{k_4}{B_4} \upsilon_{s4} \dot{\upsilon}_4 + \frac{k_5}{B_5} \upsilon_{s5} \dot{\upsilon}_{s5} \\
=& \frac{1}{B_4} e_4 (\dot{\upsilon}_r - \frac{1}{mr} \tau_L - \frac{1}{mr} \tau_R - \xi_1) + \frac{1}{B_5} e_5 (\dot{\omega}_r + \frac{l}{Ir} \tau_L \\
& - \frac{l}{Ir} \tau_R - \xi_2) \\
& + \frac{k_4}{B_4} \upsilon_{s4} [A_4 \upsilon_{s4} + (B_4 - \upsilon_{s4}) f(e_4) - (D_4 + \upsilon_{s4}) g(e_4)] \\
& + \frac{k_5}{B_5} \upsilon_{s5} [A_5 \upsilon_{s5} + (B_5 - \upsilon_{s5}) f(e_5) - (D_5 + \upsilon_{s5}) g(e_5)]
\end{aligned}
\tag{62}
$$

By substituting (57) and (58) into (62), $\dot{V}_2$ is calculated that

$$
\begin{aligned}
\dot{V}_2 =& - \frac{k_4}{B_4} e_4 \upsilon_{s4} - \frac{k_5}{B_5} e_5 \upsilon_{s5} - \frac{k_4}{B_4} \upsilon_{s4}^2 (A_4 - f(e_4) - g(e_4)) \\
& + \frac{k_4}{B_4} \upsilon_{s4} (B_4 f(e_4) - D_4 g(e_4)) - \frac{k_5}{B_5} \upsilon_{s5}^2 (A_4 - f(e_4) - \\
& g(e_4)) + \frac{k_4}{B_4} \upsilon_{s4} (B_4 f(e_4) - D_4 g(e_4))
\end{aligned}
\tag{63}
$$

Then, based on the definition of the shunting model that has been illustrated from (51) to (53), it has

$$
k_4 \upsilon_{s4} (-e_4 + f(e_4) - g(e_4)) + k_5 \upsilon_5 (-e_5 + f(e_5) - g(e_5)) = 0 \tag{64}
$$

By assuming $B_4 = D_4$ and $B_5 = D_5$, by substituting (64) into (63), $\dot{V}_2$ is rewritten as

$$
\begin{aligned}
\dot{V}_2 =& - A_4 \frac{k_4}{B_4} {\upsilon_4}^2 - A_5 \frac{k_5}{B_5} {\upsilon_5}^2 - \frac{k_4}{B_4} {\upsilon_4}^2 |e_4| - \frac{k_5}{B_5} {\upsilon_5}^2 |e_5| \\
& - \frac{\xi_1}{B_4} e_4 - \frac{\xi_2}{B_5} e_5 \\
& \leq - \frac{k_4 {\upsilon_{s4}}^2 - \xi_1}{B_4} |e_4| - \frac{k_5 {\upsilon_{s5}}^2 - \xi_2}{B_5} |e_5|
\end{aligned}
\tag{65}
$$

Then, it is obvious that whenever $k_4 {\upsilon_{s4}}^2 \geq |\xi_1|$ and $k_5 {\upsilon_{s5}}^2 \geq |\xi_2|$, the dynamics control is input to state stable. It is worth mentioning that the maximum value of υ_{s4} and υ_{s5} are B_4 and B_5, respectively. Therefore, in order to guarantee the stability, $k_4 {B_4}^2$ and $k_5 {B_5}^2$ have to be set larger than d_1 and d_2, respectively.

It is proved that the dynamic control is input to state stable, thus, e_η is bounded, since the kinematic control is asmptotically stable, it is concluded that the control design is input to state stable.

Remark 4 The bioinspired sliding mode control is robust to disturbances and free from chattering. The output of the shunting models υ_{s4} and υ_{s5} are strictly bounded between $(-D_4, B_4)$ and $(-D_5, B_5)$. In addition, the control smoothness of the torque control inputs is critical in real applications, the proposed bioinspired control is a feasible solution that provides the smooth control inputs under both disturbances and noises, thus more effective than conventional design.

4.3 SIF and ESIF

It is necessary for mobile robot equips with efficient and effectiveness filters that is capable of proving accurate state estimates because the autonomous robot often operates in hard conditions where system and measurement noises have huge impact on the control performance. Therefore, the ASIF and AESIF are applied to provide accurate sate estimates under modelling uncertainties. Considering the working conditions of the autonomous system, having a filter with more robustness is rather critical in real world applications.

First the design of the ASIF is used to provide accurate velocity estimates, the predicting stage is followed by three main equations as

$$\hat{\Omega}_{a,k+1|k} = F\hat{\Omega}_{a,k|k} + B_\tau \tau_{c,k} \tag{66}$$

$$P_{k+1|k} = FP_{k|k}F^T + R_1 \tag{67}$$

$$\tilde{z}_{a,k+1|k} = \tilde{\Omega}_{a,k+1} - H\hat{\Omega}_{k+1|k} \tag{68}$$

where $\hat{\Omega}_{a,k|k}$ is the posterior velocity estimates that is defined as $\hat{\Omega}_{a,k|k} = \begin{bmatrix} \hat{\upsilon}_{a,k|k} & \hat{\omega}_{a,k|k} \end{bmatrix}^{\mathrm{T}}$; $\hat{\Omega}_{k+1|k}$ is the priori velocity estimates; F is the system matrix that is an 2×2 identity matrix; B_τ is the time step Δt; R_1 is the dynamic system noises covariance; $P_{k+1|k}$ is the predicted state error state error covariance; H is the measurement matrix. Then, based on the robot dynamics that is given in (5) and (7), the system model F is defined as a 2×2 identity matrix, and

$$\hat{\Omega}_{a,k+1|k} = \begin{bmatrix} \hat{\upsilon}_{a,k+1|k} \\ \hat{\omega}_{a,k+1|k} \end{bmatrix} = \begin{bmatrix} \hat{\upsilon}_{a,k|k} \\ \hat{\omega}_{a,k|k} \end{bmatrix} + \bar{M}^{-1}\bar{B}\tau_{c,k}\Delta t \tag{69}$$

where $\gamma_{1,k}$ is the system noises at time step k. The update stage is followed by the predicting stage, which are given as

$$K_{k+1} = C^{+}\mathrm{diag}(\mathrm{sat}\left(\frac{\left|\hat{\mathrm{z}}_{\mathrm{k+1|k}}\right|}{\alpha_{\mathrm{k+1}}}\right) \tag{70}$$

$$\alpha_{k+1} = S_{k+1}(S_{k+1} - Q_1)^{-1}\mathrm{diag}\left|\hat{z}_{k+1|k}\right| \tag{71}$$

$$\hat{\Omega}_{a,k+1|k+1} = \hat{\Omega}_{a,k+1|k} + K_{k+1}\hat{z}_{k+1|k} \tag{72}$$

$$\begin{aligned} P_{k+1|k+1} = (I - K_{k+1}H)P_{k+1|k}(I- \\ K_{k+1}H)^T + K_{k+1}Q_1{K_{k+1}}^T \end{aligned} \tag{73}$$

where $P_{k+1|k+1}$ is the updated state error covariance; $\hat{x}_{k+1|k+1}$ is the updated state estimates; K_{k+1} is the updated sliding innovation gain; Q_1 is the measurement noises covariance; and α_{k+1} is the sliding boundary. The linear model of the ASIF is used to provide accurate state estimates of the velocities under noises and modeling uncertainties.

After the ASIF for the dynamics of the mobile robot is designed, the AESIF is then designed to provide accurate position state estimates, the procedure is similiar to the extended Kalman filter, which requires linearization of the system model. First, define $P = \begin{bmatrix} x & y & \theta \end{bmatrix}^T$, the predicting stage is given as

$$\hat{P}_{a,k+1|k} = f(\hat{P}_{a,k}, \tau_k) \tag{74}$$

$$S_{k+1|k} = F_{f,k}S_{k|k}F_{f,k}^T + R_2 \tag{75}$$

$$\tilde{P}_{a,k+1|k} = P_{a,k+1} + H_f(\hat{P}_{a,k+1|k}) \tag{76}$$

where $\hat{P}^{-}_{a,k+1|k}$ is the priori state estimates; $F_{f,k}$ is the linearized function of $f(\hat{P}_{a,k|k}, u_k)$; and R_2 is the system noises covariance in the position estimates; $\tilde{P}_{k+1|k}$ is the innovation; $P_{a,k+1}$ is the position measurement; $H_f(\hat{P}_{k+1|k})$ is the measurement function; $S_{k+1|k}$ is the predicted state error covariance. Based on (5), the nonlinear system model $f(\hat{P}_{k|k}, \tau_k)$ is given as

$$\begin{bmatrix} \hat{x}_{a,k+1|k} \\ \hat{y}_{a,k+1|k} \\ \hat{\theta}_{a,k+1|k} \end{bmatrix} = \begin{bmatrix} \hat{x}_{a,k|k} + (\cos\hat{\theta}_{a,k|k}\hat{\upsilon}_{a,k|k})\Delta t \\ \hat{y}_{a,k|k} + (\sin\hat{\theta}_{a,k|k}\hat{\upsilon}_{a,k|k}\Delta t \\ \hat{\theta}_{a,k|k} + \hat{\omega}_{a,k|k}\Delta t \end{bmatrix} \tag{77}$$

Then, the updating stage of the AESIF would be identical to the linear model of the ASIF that is provided from (70) to (73) with F and H are respectively replaced with linearzied system and measurement functions. The stability of the sliding innovation filter has been proven in,[31] thus the estimation error is assumed to be bounded in order for the design of the controller.

Remark 5 Compared with KF and EKF, the design of the ASIF and AESIF of the mobile robot aims to address the problem when modelling error occurs due to ill conditioned robot that sends faulty modelling data to the filter, and provide accurate state estimates as well. In general, the proposed filters have two different working conditions, when there is no modelling uncertainties, accurate state estimates that is identical to KF and EKF would be generated. Under modelling uncertainties, the sliding boundary would be set to a fixed value that restricts the gain, thus acting more like a sliding mode observer to provide relatively more accurate state estimates.

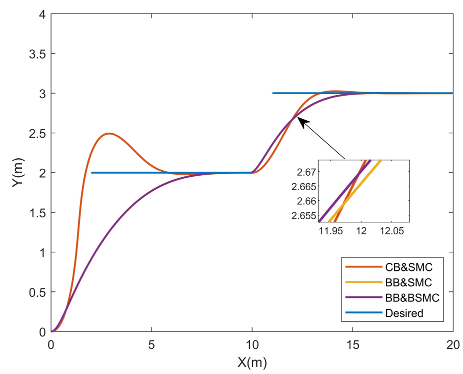

Figure 3. Tracking performance of different tracking method for a discrete straight path. CB: Conventional Backstepping Control; SMC: Sliding Mode Control; BB: Bioinspired Backstepping Control; BSMC: Bioinspired Sliding Mode Control

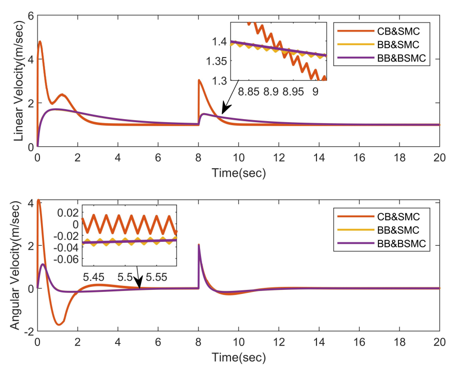

Figure 4. Velocity control signal of tracking a discrete straight path.

5. RESULTS

This section presents multiple simulation results that demonstrate the efficiency and effectiveness of the proposed control strategy. The proposed hybrid tracking method along with ASIF and AESIF is used to track various trajectories. The sampling time is set to be 0.01 seconds. The initial state covariance of the ASIF and AESIF are set to be $P_{(0|0)} = 10R$ and the measurement matrix for the kinematics and dynamics of the mobile robot are respectively defined as 3 by 3 and 2 by 2 identity matrices. The mass of the mobile robot is set to $m = 5$ and moment of inertia $I = 0.1$, $l = 1$, and the radius of the left and right wheels are both defined as $r = 0.5$. The parameters of the shunting model in kinematic control are treated as $k_1 = 1$, $A_1 = 4$, $B_1 = D_1 = 2$, while the control parameters for the bioinspired dynamic control are set to be $k_4 = k_5 = 1$, $A_4 = A_5 = 8$, and $B_4 = B_5 = D_4 = D_5 = 4$. To further reduce the initial torque demand, the desired linear velocity at initial

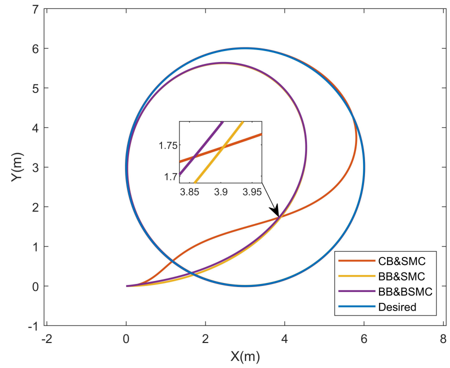

Figure 5. Tracking performance of different tracking method for a circular path.

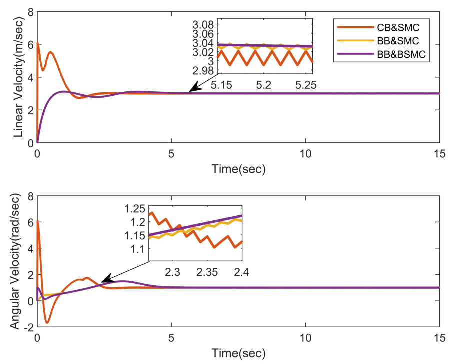

Figure 6. Velocity control signal of tracking a circular path.

stage is defined as υ_d=$\upsilon_\mathrm{d}(1-e^{-t/0.5})$. In comparison, the control parameters for the conventional backstepping and sliding mode control are set to $k_1 = k_2 = k_3 = 2$; $C_4 = C_5 = 2$, respectively. In order to calculate the performance of the estimation accuracy, the root mean square error (RMSE) is calculated as

$$\mathrm{RMSE} = \sqrt{\sum_{i=1}^{n} \frac{\left(\tilde{W} - W\right)^2}{n}} \tag{78}$$

where $\tilde{W}$ and W are respectively the estimated and actual states of the mobile robot.

5.1 Tracking performance of the bioinspired control

The proposed control strategy is firstly tested and compared in a situation where there are no system or measurement noises. There are two different desired paths are tested. The mobile robot initial position for both scenarios are defined as $(0, 0)$. The desired path is defined $x = 2 + t$ and $y = 2$ for the first 8 seconds, after 8 seconds, the trajectory changes to $x = 11 + t$ and $y = 3$, thus the initial tracking error is $(2, 2)$ and another tracking error of $(0, 1)$ at 8 seconds. As can be seen from 3, all the control methods tracks its desired straight path, however, by observing the velocity graph in Figure 4, it can be found that there is a linear velocity jump at the initial stage and during the sudden change of the path from the conventional methods. This linear velocity jump implies that the initial torque demand would tend to be large to reach such velocity instantly at the initial stage, which makes the conventional backstepping method not practical, However, the proposed bioinspired hybrid control method avoids this unrealistic velocity jump issue and subsequently reduces the velocity overshoot as well. In addition, the sliding mode chattering issue has been avoided as can be observed from the zoom in picture from Figure 4, the bioinspired sliding mode torque control provides smooth velocity curve without chattering. To further demonstrate that the proposed controller is capable of tracking a curved path, the proposed method is

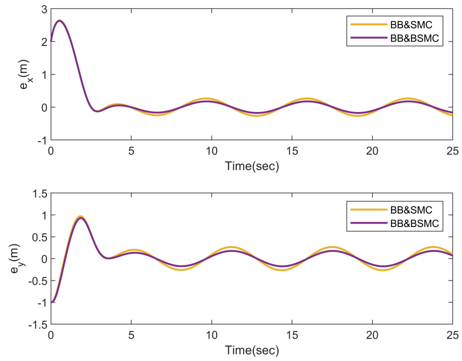

Figure 7. Tracking error under disturbances.

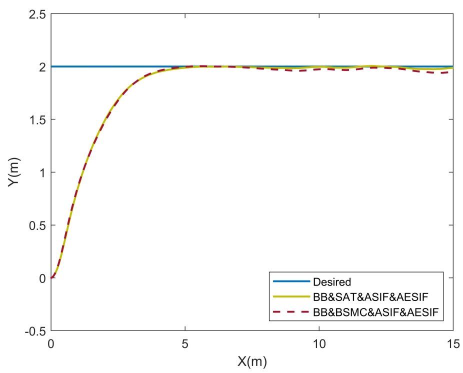

Figure 8. Position estimates of different tracking methods for a straight path under noises. SAT: Sliding mode control with saturation function

used to track a desired circular path is defined as $x = 3 + 3\cos(-\pi/2 + t)$ and $y = 3 + 3\sin(-\pi/2 + t)$, Figure 5 and 6 shows that the speed jump issue is also avoided as well.

To demonstrate the robustness of the proposed control under disturbances, the proposed tracking method is used to track a desired path which is provided in Figure 5. It can be seen in Figure 7, the conventional sliding mode control that are provided in (55) and (61) yield larger tracking error while the proposed tracking method has lower maximum tracking error at steady state. In addition, by adjusting A in the shunting model, the steady state error could be further lowered at steady state.

5.2 Tracking performance under noises

The proposed bioinspired dynamic control strategy is capable of providing smooth control torque input even with large noises that occurs within the dynamics of the mobile robot. The noise covariance is set to be $R_2 = Q_2 = \mathrm{diag}[1.5\mathrm{e}^{-4}, 1\mathrm{e}^{-4}]$ and the noise covariances for the kinematics are set to be $R_1 = Q_1 = \mathrm{diag}[2\mathrm{e}^{-8}, 2\mathrm{e}^{-8}, 1^{-8}]$. The desired trajectory is set to be $X_d = t$ and $Y_d = 2$, the results is seen in Figure 8 and 9, it can be seen that both methods are able to track its desired trajectory, however, by observing the torque control command in Figure 9, it is seen that the bioinspired sliding mode control yield smooth torque control command even with the presence of the system noises. Although the saturation method eliminates the chattering issue in conventional sliding mode control design, when facing noises, the torque control command is not smooth, which is undesirable in real world applications, making the proposed bioinspired hybrid strategy a better choice.

5.3 State estimation under faulty conditions

As for the estimation accuracy, under normal conditions where no modelling error is presented, the ASIF and AESIF provides almost identical state estimates as the KF and UKF does, which is observed in Figure 1. However, since the mobile robots usually work in complex environments, the equipped estimators could fail,

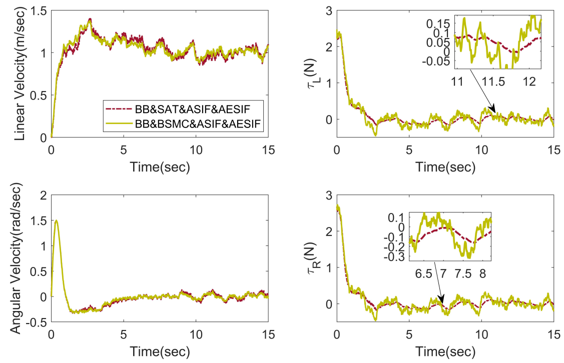

Figure 9. Velocity estimates and toque control command of tracking a straight path under noises.

Table 1. RMSE under normal case

States	KF and UKF	ASIF and AESIF
Linear velocity	9.7×10^{-3}	9.7×10^{-3}
Angular velocity	2.5×10^{-3}	2.5×10^{-3}
X	1.3×10^{-4}	1.3×10^{-4}
Y	1.3×10^{-4}	1.3×10^{-4}
θ	8.5×10^{-4}	8.5×10^{-4}

which will highly affect the accuracy of the tracking performance and potentially make the entire system fail. The ASIF and AESIF are capable of providing accurate state estimates and robust to modelling uncertainties. To validate the robustness of the proposed estimators. There are faults injected to the filters due to modelling error, at 4 seconds time point, the kinematic model that is processed by the filters is changed to

$$\begin{bmatrix} \hat{x}^-_{a,k+1} \\ \hat{y}^-_{a,k+1} \\ \hat{\theta}^-_{a,k+1} \end{bmatrix} = \begin{bmatrix} 1.5\hat{x}_{a,k} + (\cos\hat{\theta}_{a,k}\hat{\upsilon}_{a,k})\Delta t \\ 1.5\hat{y}_{a,k} + (\sin\hat{\theta}_{a,k}\hat{\upsilon}_{a,k}\Delta t \\ 1.2\hat{\theta}_{a,k} + \hat{\omega}_{a,k}\Delta t \end{bmatrix} \tag{79}$$

then, after 12 seconds, the dynamic model that is processed by the filters is changed to

$$\hat{\Omega}^-_{k+1} = \begin{bmatrix} \hat{\upsilon}^-_{r,k+1} \\ \hat{\omega}^-_{r,k+1} \end{bmatrix} = \begin{bmatrix} 1.5\hat{\upsilon}_{r,k} \\ -1.5\hat{\omega}_{r,k} \end{bmatrix} + \bar{M}^{-1}\bar{B}\tau_{c,k}\Delta t + \gamma_k \tag{80}$$

Table 2 shows the RMSE between different filtering strategies, under modelling error, the KF and UKF will fail to provide accurate results, while the proposed filtering strategy provides better state estimates, which is crucial for the control to work properly.

Remark 6 It is worth mentioning that the estimation error that occurs within the kinematic of the mobile robot has huge impact on the control effectiveness. At the time point of 4 seconds, the incorrect reading of the velocity will cause the demanding torque surge, which is impossible for the mobile robot to reach. Thus, having the AESIF to estimate the posture of the mobile robot has apparent advantage over the UKF as such impractical torque surge issue has been avoided.

Table 2. RMSE under faulty case

States	KF and UKF	ASIF and AESIF
Linear velocity	1.1×10^{-1}	1.1×10^{-2}
Angular velocity	1.6×10^{-2}	1.1×10^{-2}
X	1.1×10^{-2}	1.4×10^{-4}
Y	6.0×10^{-3}	1.2×10^{-4}
θ	2.1×10^{-4}	2.0×10^{-4}

6. CONCLUSION

In this paper, a bioinspired hybrid control strategy of a mobile robot is proposed, then it is integrated with ASIF and AESIF to provide accurate state estimate. The shunting model that is used in this paper is discovers to have excellent characteristic as it provide bounded output and also acting as a low pass filter. These special characteristics allow the control performance to be smooth and bounded. In addition, considering the modeling error and uncertainties, ASIF and AESIF are used to provide accurate state estimates while remaining its robustness.

REFERENCES

[1] Chwa, D., "Tracking Control of Differential-Drive Wheeled Mobile Robots Using a Backstepping-Like Feedback Linearization," *IEEE Transactions on Systems, Man, and Cybernetics - Part A: Systems and Humans* **40**(6), 1285–1295 (2010).

[2] Benchouche, W., Mellah, R., and Bennouna, M. S., "The impact of the dynamic model in feedback linearization trajectory tracking of a mobile robot," *Periodica polytechnica Electrical engineering and computer science* **65**(4), 329–343 (2021).

[3] Nie, J., Wang, Y., Miao, Z., Jiang, Y., Zhong, H., and Lin, J., "Adaptive fuzzy control of mobile robots with full-state constraints and unknown longitudinal slipping," *Nonlinear Dynamics* **106**(4), 3315–3330 (2021).

[4] Lee, S. and Chwa, D., "Dynamic Image-Based Visual Servoing of Monocular Camera Mounted Omnidirectional Mobile Robots Considering Actuators and Target Motion via Fuzzy Integral Sliding Mode Control," *IEEE Transactions on Fuzzy Systems* **29**(7), 2068–2076 (2021).

[5] Chen, Z., Liu, Y., He, W., Qiao, H., and Ji, H., "Adaptive-Neural-Network-Based Trajectory Tracking Control for a Nonholonomic Wheeled Mobile Robot with Velocity Constraints," *IEEE Transactions on Industrial Electronics* **68**(6), 5057–5067 (2021).

[6] Ding, L., Li, S., Gao, H., Chen, C., and Deng, Z., "Adaptive Partial Reinforcement Learning Neural Network-Based Tracking Control for Wheeled Mobile Robotic Systems," *IEEE Transactions on Systems, Man, and Cybernetics: Systems* **50**(7), 2512–2523 (2020).

[7] Li, S., Ding, L., Gao, H., Liu, Y. J., Li, N., and Deng, Z., "Reinforcement Learning Neural Network-Based Adaptive Control for State and Input Time-Delayed Wheeled Mobile Robots," *IEEE Transactions on Systems, Man, and Cybernetics: Systems* **50**(11), 4171–4182 (2020).

[8] Ren, C., Li, X., Yang, X., and Ma, S., "Extended state observer-based sliding mode control of an omnidirectional mobile robot with friction compensation," *IEEE Transactions on Industrial Electronics* **66**(12), 9480–9489 (2019).

[9] Lin, L., Wu, P., He, B., Chen, Y., Zheng, J., and Peng, X., "The sliding mode control approach design for nonholonomic mobile robots based on non-negative piecewise predefined-time control law," *IET Control Theory and Applications* **15**(9), 1286–1296 (2021).

[10] Zhu, D. and Sun, B., "The bio-inspired model based hybrid sliding-mode tracking control for unmanned underwater vehicles," *Engineering Applications of Artificial Intelligence* **26**(10), 2260–2269 (2013).

[11] Yang, S. X., Zhu, A., Yuan, G., and Meng, M. Q., "A Bioinspired Neurodynamics-Based Approach to Tracking Control of Mobile Robots," *IEEE Transactions on Industrial Electronics* **59**(8), 3211–3220 (2012).

[12] Zhang, X., Wang, R., Fang, Y., Li, B., and Ma, B., "Acceleration-Level Pseudo-Dynamic Visual Servoing of Mobile Robots with Backstepping and Dynamic Surface Control," *IEEE Transactions on Systems, Man, and Cybernetics: Systems* **49**(10), 2071–2081 (2019).

[13] Rahimnejad, A., Enayati, J., Vanfretti, L., Gadsden, S. A., and Alshabi, M., "Reinforced Lattice Kalman Filters: A Robust Nonlinear Estimation Strategy," *IEEE Open Journal of Signal Processing* **4**(August), 410–423 (2023).

[14] Zhang, H., Zhou, X., Wang, Z., and Yan, H., "Maneuvering Target Tracking with Event-Based Mixture Kalman Filter in Mobile Sensor Networks," *IEEE Transactions on Cybernetics* **50**(10), 4346–4357 (2020).

[15] Zhu, P. and Ren, W., "Fully Distributed Joint Localization and Target Tracking With Mobile Robot Networks," *IEEE Transactions on Control Systems Technology* **29**(4), 1519–1532 (2020).

[16] Goodman, J., Hilal, W., Gadsden, S. A., and Eggleton, C. D., "Adaptive SVSF-KF estimation strategies based on the normalized innovation square metric and IMM strategy," *Results in Engineering* **16**(October), 100785 (2022).

[17] Aissa, B. C. and Fatima, C., "Neural networks trained with Levenberg-Marquardt-Iterated Extended Kalman Filter for mobile robot trajectory tracking," *Journal of Engineering Science and Technology Review* **10**(4), 191–198 (2017).

[18] Cao, H. Q., Nguyen, H. X., Tran, T. N. C., Tran, H. N., and Jeon, J. W., "A Robot Calibration Method Using a Neural Network Based on a Butterfly and Flower Pollination Algorithm," *IEEE Transactions on Industrial Electronics* **69**(4), 3865–3875 (2022).

[19] Xu, Z., Yang, S. X., and Gadsden, S. A., "Enhanced Bioinspired Backstepping Control for a Mobile Robot With Unscented Kalman Filter," *IEEE Access* **8**, 125899–125908 (2020).

[20] Partovibakhsh, M. and Liu, G., "An adaptive unscented kalman filtering approach for online estimation of model parameters and state-of-charge of lithium-ion batteries for autonomous mobile robots," *IEEE Transactions on Control Systems Technology* **23**(1), 357–363 (2015).

[21] He, X., Su, Y., and Qiu, Y., "An Improved Unscented Kalman Filter for Maneuvering Target Tracking*," *Journal of Physics: Conference Series* **2216**(1), 012010 (2022).

[22] Zhai, J. y. and Song, Z. b., "Adaptive sliding mode trajectory tracking control for wheeled mobile robots," *International Journal of Control* **92**(10), 2255–2262 (2019).

[23] Abid, H., "Takagi-Sugeno Fuzzy Controller and Sliding Mode Controller for a Nonholonomic Mobile Robot," *Mathematical Problems in Engineering* **2021**, 1–10 (2021).

[24] Nagpal, K. and Khargonekar, P. P., "Filtering and smoothing in an H sup infinity setting," *IEEE Transactions on Automatic Control* **36**(2), 152–166 (1991).

[25] Bernstein, D. S. and Haddad, W. M., "Steady-state Kalman filtering with an H error bound," *Systems & control letters* **12**(1), 9–16 (1989).

[26] Li, B., Lu, Y., and Karimi, H. R., "Adaptive fading extended kalman filtering for mobile robot localization using a doppler–azimuth radar," *Electronics (Switzerland)* **10**(20), 1–18 (2021).

[27] Enayati, J., Rahimnejad, A., Vanfretti, L., Gadsden, S. A., and Al-Shabi, M., "Dynamic Harmonic Estimation Using a Novel Robust Filtering Strategy: Iterated Sliding Innovation Cubature Filter," *IEEE Transactions on Instrumentation and Measurement* **72**, 1–10 (2023).

[28] Lee, A. S., Hilal, W., Andrew Gadsden, S., and Al-Shabi, M., "Combined Kalman and sliding innovation filtering: An adaptive estimation strategy," *Measurement: Journal of the International Measurement Confederation* **218**(October 2022), 113228 (2023).

[29] Xu, Z., Gadsden, S. A., Yang, S. X., and Su, C.-y., "A Novel Tracking Control for Mobile Robot Based on Bioinspired Neurodynamics," in [*8th International Conference on System and Control*], (2019).

[30] Yang, S. X. and Meng, M., "An efficient neural network approach to dynamic robot motion planning," *Neural Networks* **13**(2), 143–148 (2000).

[31] Andrew Gadsden, S. and Al-Shabi, M., "The Sliding Innovation Filter," *IEEE Access* **8**, 96129–96138 (2020).